Design and fabrication of thin-film spatial filter

Ying Zhang (章 瑛)[1,2*], Hongji Qi (齐红基)[1], Kui Yi (易 葵)[1], Yanzhi Wang (王胭脂)[1], Hongbo He (贺洪波)[1], and Jianda Shao (邵建达)[1]

[1]*Key Laboratory of Materials for High Power Laser, Shanghai Institute of Optics and Fine Mechanics, Chinese Academy of Sciences, Shanghai 201800, China*

[2]*Graduate School of the Chinese Academy of Sciences, Beijing 100039, China*

[*]*Corresponding author: zhangying0127@163.com*

Received March 14, 2014; accepted May 3, 2014; posted online September 10, 2014

The combination of lens and pinhole limits the enhancement of the laser output power in the high-power laser system. Low-pass spatial filter without focusing can surmount the drawbacks of the pinhole filters. The low-pass spatial filters based on multilayer dielectric film are analyzed and their filtering performances are validated. The non-focusing low-pass spatial filter is successfully explored to substitute for the focusing one. The design method is based on phase-shifted Rugate thin-film spatial filter, narrow bandpass filter and the combined device of long-wave-pass and short-wave-pass cutoff filters, and the angular spectrum bandwidth of bandpass filter are up to submillimeter radians. We mainly discuss three design methods and point out their advantages and disadvantages to find out the best one. The experimental results show that the effects of random and system error during depositing the filter is mainly responsible for the deviation of the designed and measured values.

OCIS codes: 050.5080, 310.6860, 330.6110.

doi: 10.3788/COL201412.S20501.

In the high-power laser system, the pinhole spatial filter is widely used for beam cleanup, its requisite focusing of the laser beam presents poor functionality[1]. The energy intensity at the focal plane of the pinhole filter is more than 10^{12} W/cm^2. So the plasma closure may be probably caused and the material of the pinhole plate is easily burned[2,3]. As a hard-edge diaphragm, the low-frequency diffractive rings are likely to appear[4,5]. The spatial filter has the advantages of filtering out the rapid growing non-linear components of spatial frequency, and effectively improving the beam quality and so on[6–15]. Spatial filter is an important optical application of the thin-film technology. Non-focusing spatial filtering technique bases on multilayer dielectric film. By the matrix transfer method, the diffraction efficiencies, angular spectrum bandwidths, and the light spectrum bandwidths of multilayer dielectric film are analyzed. The combination thin-film has better spatial filtering performance than that of the combination of lens and pinhole. We design the spatial filtering is using three different methods and analyze their advantages and disadvantages. Finally, we find out the best optimized method and the film is deposited by ion-beam sputtering technique. The microstructure, composition, and optical properties have been investigated by scanning electron microscopy (SEM) and spectrophotometer. The result shows that the film has optically flat and uniform surface and the structure of the film is compact. The result also shows that the transmittance can be attenuated by the absorption of materials, thickness errors, and refractive index inhomogeneity in the process of the film depositing. At the same time, the course of manufacturing the film is needed to be controlled accurately in order to gain result which is consistent with the calculated results.

The principle of phase-shifted Rugate thin-film spatial filter is the left and right sides of the two Rugate films having angular spectrum selectivity to the incident light. The left and right sides of the two Rugate films consist of Fabry–Perot chamber for choosing the angle spectrum. The low-frequency component of the angular spectrum is efficiently transmitted Rugate film due to the interference effects of Fabry–Perot filter, while the high-frequency component of the angular spectrum is reflected by Fabry–Perot filter to realize the beam spatial low-pass filtering.

The principle of phase-shifted Rugate thin film is based on the Fabry–Perot filter. The two side reflective film of Fabry–Perot cavity is instead used by Rugate thin film in order to get sharper and smoother transition from bandpass to cut-off of the bandpass filter. Figure 1 shows a schematic diagram of transmission and reflection and that the monochromatic plane wave

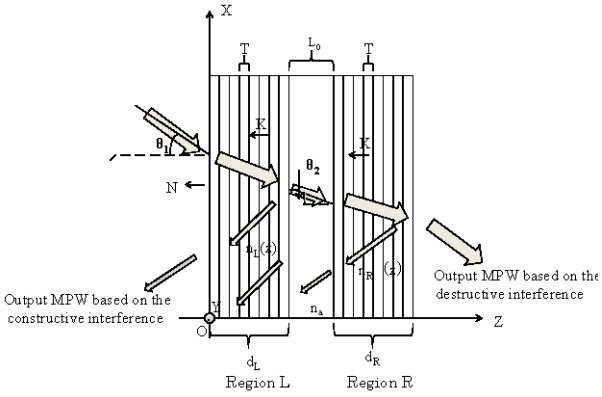

Fig. 1. Schematic diagram phase-shifted Rugate spatial filter of the transmission and reflection of MPW.

(MPW) is obliquely incident upon Rugate phase shift film.

XYZO is a Cartesian coordinate system. T and N denote grating period and unit vector normal to the front surface of the film, respectively, d_{L} and d_{R} represent both sides of the film thickness, respectively, L_0 represents the equivalent optical path causing phase hop, n_0 and n_{G} represent the refractive indexes of air and substrate, respectively, and $n_{\mathrm{L}}(z)$ and $n_{\mathrm{R}}(z)$ denote refractive indexes of the left and the right films, respectively. The refractive index is expressed as

$$n_{\mathrm{L}}(z) = n_a + n_{\mathrm{p}} \sin\left(Kz + \Phi_{\mathrm{GL}}\right), \tag{1}$$

$$n_{\mathrm{R}}(z) = n_a + n_{\mathrm{p}} \sin\left[K\left(z - d_L - L_0\right) + \Phi_{\mathrm{GR}}\right], \tag{2}$$

where n_{p} is the difference of the refractive index modulation of the left and right sides the phase-shift film, Φ_{GL} and Φ_{GR} are initial phase of the left and right sides of the film, respectively. K denotes the grating's vector, the module of which is $2\pi/T$.

Transmittance spectrum and angular spectrum of phase-shift Rugate thin-film spatial filter are calculated according to parametric value of simulation phase-shift Rugate coating, which is listed in Table. 1.

Figure 2 shows the designed results of a phase-shift film Rugate spatial filter, and the angular resolution of the filter is defined as a half of angular spectrum of the peak width. The results show that the angular resolution of the phase-shift Rugate spatial filter reaches to submillimeter radians.

Figure 3 shows the electric field in the designed phase-shift Rugate spatial filter. It is found that the Fabry–Perot chamber trap the main electric field at a center wavelength of 1064 nm and the electric field value is up to 11000 V/m, which is a very miraculous number.

Table. 1. Parametric Values of Simulation Phase-shift Rugate Coating

Parameter	Value	Parameter	Value
T	350 nm	L_0	175 nm
λ_0	1064 nm	n_{G}	1.5
n_0	1.00	n_a	1.6
θ_1	0.5233 rad		

The coating stacks of narrow bandpass filters are named Sub|(HL)^{24}H2L(HL)^{24}HL(HL)^{24}H2L(HL)^{24}H|Air. "Sub" denotes substrate, "Air" denotes air, and "H" and "L" denote Nb_2O_5 (2.20) and SiO_2 (1.45535), respectively. Each symbol represents an optical thickness of one-quarter wavelength at 1053 nm.

Figure 4 shows the angular spectrum of the designed narrow bandpass filter, which provides angular resolution with 0.28 mrad at a center wavelength of 1053 nm.

Figure 5 shows the electric field distribution in the designed narrow bandpass filter. It is found that the 2L layers trap the main electric field at a center wavelength of 1053 nm and the electric field value is up to 10^8 V/m.

The combined device is composed of long-wave-pass and short-wave-pass cutoff filters, which is designed using the steep side of the minus filters. The long-wave-pass and short-wave-pass cutoff filters are, respectively, designed with the following starting layer structure: glass/(0.7598H0.7638L0.32345H)^1(0.32345H0.6635L0.4135H)^{1}0.97(0.3655H0.73L0.3655H)^3(0.3655H0.73L0.3655H)^{60} 0.99(0.3655H0.73L0.3655H)^7(0.7925H0.8713L0.2796H)^1(0.2796 H0.2999L0.37925H)^1(0.37925H0.8850L0.8245H)^1/air and glass/(0.8309H0.9003L0.4155H)^1(0.4155H0.9002L0.8333H)^1 (0.5HL0.5H)^1 (0.5HL0.5H)^{50}1.02(0.5HL0.5H)^3 (0.6429H0.9041L 0.4237H)^1(0.4237H2.1188L)^1/air.

The long-wave-pass and short-wave-pass cutoff filters consist of 153 and 118 quarter-wave optical thickness (QWOT) layers, respectively. Angular spectrum of the designed long-wave-pass and short-wave-pass cutoff filters is illustrated in Fig. 6. and provides about 99% transmittance with a half of angular spectrum of the peak width 2.8 mm rad at a center wavelength of 1053 nm.

Figure 7 shows the electric field distribution in the long-wave-pass. It is found that the middle layers trap the main electric field at a center wavelength of 1053 nm and the electric field value is only to 15 V/m.

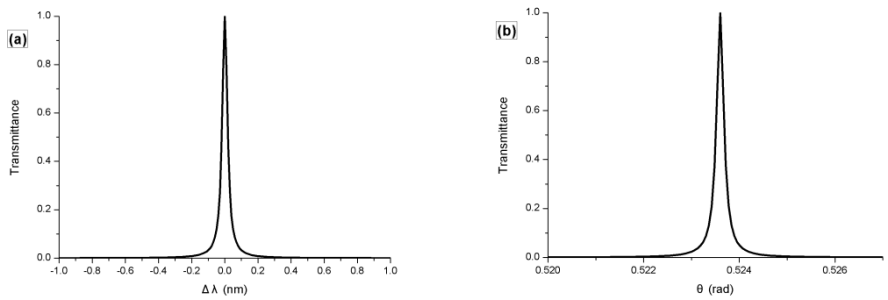

Fig. 2. (a) Transmittance spectrum and (b) angular spectrum of phase-shift Rugate filter in 40 T.

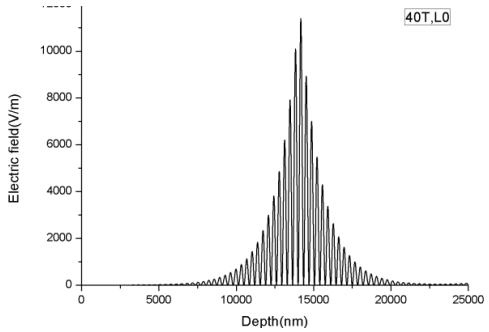

Fig. 3. Electric field distribution of phase-shift Rugate spatial filter.

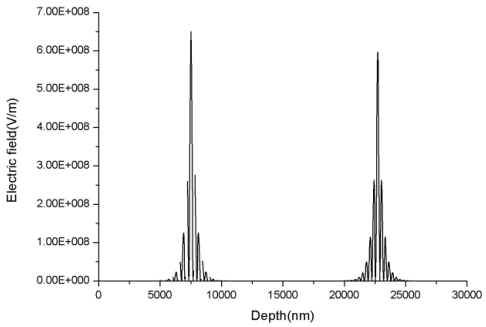

Fig. 5. Electric field distribution of the designed narrow bandpass filter.

From the above it can be seen that three designs have their own advantages and disadvantages. Coating structure of the phase-shifted Rugate thin-film spatial filter and narrow bandpass filter is relatively simple, but the electric field is too high to be suitable for fabrication, while the electric field of the combined device of long-wave-pass and short-wave-pass cutoff filters is much lower than the former. So the combined device of long-wave-pass and short-wave-pass cutoff filters can be chosen.

The combined device of long-wave-pass and short-wave-pass cutoff filters has been deposited on BK7 substrate using the ion-beam sputtering technique. In the experiment, the long-wave-pass filter was fabricated. We provide a high production accuracy of the layers by control the depositing time. The pressure in the vacuum tank was pumped by turbo-molecular pumps to 1×10^{-5} Pa before deposition. The gas pressure was 1×10^{-2} Pa and temperature was 80 °C during the deposition process. The film was deposited at a rate of 0.2 nm s^{-1}. The purity of the Ta and SiO_2 target were both 99.999%. Ultrahigh purity O_2(99.99%) was used to react with Nb generated by the Nb target to form Nb_2O_5.

The cross-sectional microstructure was observed by the field emission SEM with a Zeiss Auriga microscope. The transmission spectra of the coatings were measured by a Lambda 900 spectrophotometer in the 1000–1200 nm spectral range.

Figure 8 shows the transmission spectra of designed and measured long-wave-pass cutoff filter. The designed filter has an average transmittance of 99% in the wavelength range 1030–1080 nm, as indicated by the dotted line in Fig. 8. It can be seen that the maximum value of the measured spectrum transmittance only reach to 70%. The deviations are due to manufactured errors rather than measurement errors, because the effect of system errors and random errors can be introduced in the physical thickness and refractive index during the manufacturing process.

Figure 9 shows that the thin-film layer is SiO_2 and the thicker one is Nb_2O_5, and the film has optically flat and uniform surface and the structure of the film is compact. Micrograph shown in Fig. 9 demonstrates that the manufactured errors lead to deviations of the measured spectrum transmittance curve from the design one. Therefore, the reasons for errors made during deposition are important for the manufacturing of long-wave-pass cutoff filter.

The reasons that produce the layer thickness errors are analyzed. First, if the voltage and current are

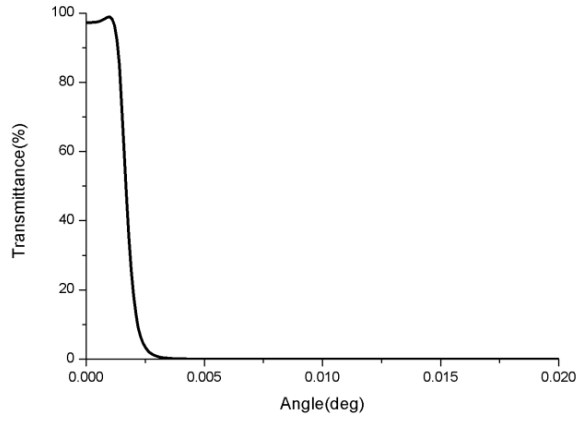

Fig. 4. Angular spectrum of the designed narrow bandpass filter.

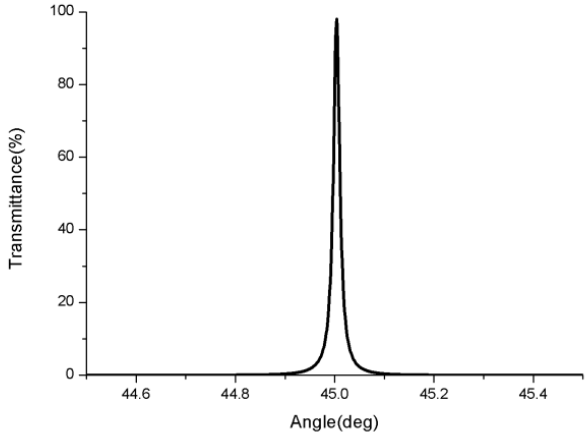

Fig. 6. Angular spectrum of the designed long-wave-pass and short-wave-pass cutoff filters.

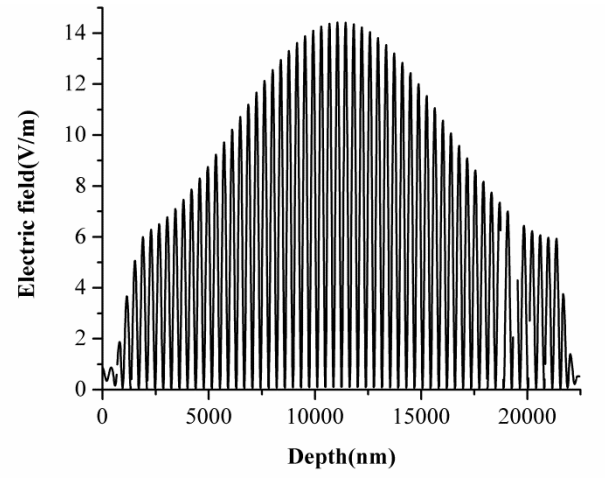

Fig. 7. Electric field distribution of cut-off filter combination device.

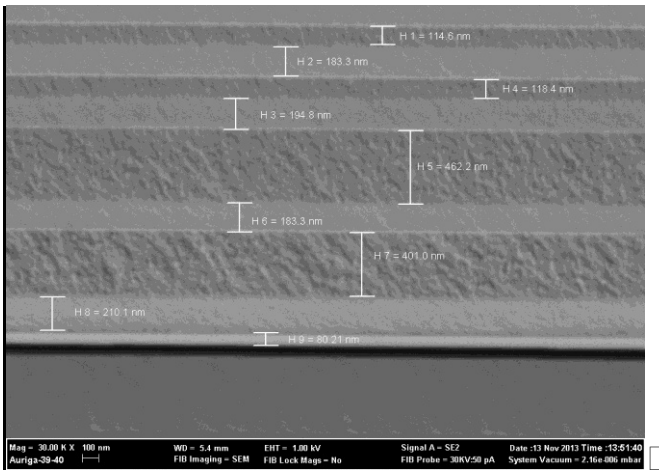

Fig. 9. Scanning electron micrograph and measured layer thickness (nm) of long-wave-pass cutoff filter.

unstable, the deposition rate of coating materials is unstable, so the estimations of mean deposition are inaccurate. Therefore, the deposition rate is different and the thickness deviates from the designed value.

In conclusion, we design a thin-film spatial filter by three different methods and combination devices spatial filter obtains a better design results. The fabrication of the thin-film spatial filter from two sources of materials can be accomplished by the ion-beam sputtering method. The experimental results show the feasibility of fabrication spatial filter combination device, but there are some errors. Future work will focus on realizing more excellent spatial filter designs and reducing random error and system error and controlling precision during the process of depositing the filter.

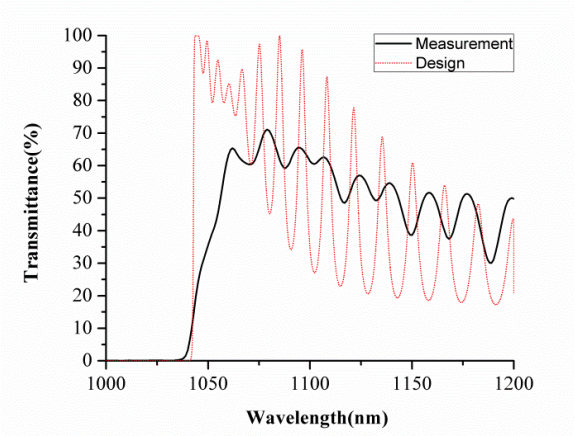

Fig. 8. Transmission spectra of designed and experimental measurements for short-wave-pass cutoff filter.

References

1. G. Zheng, B. Shen, J. Tan, Y. He, and X. Wang, Chin. Opt. Lett. **9,** 030501 (2011).
2. F. Wang, Q. Zhu, D. Jiang, Q. Zhang, H. Liu, Z. Peng, and X. Tang, Laser J. **26,** 19 (2005).
3. X. Zhang, Q. Yuan, J. Zhao, D. Hu, W. Dai, W. Zhou, X. Jiang, W. Deng, and K. Zhang, High Power Laser Part. Beams **22,** 2921 (2010).
4. Y. Gao, B. Zhu, D. Liu, X. Liu, and Z. Lin, Appl. Opt. **48,** 1591 (2009).
5. Y. Gao, B. Zhu, D. Liu, X. Liu, and Z. Lin, J. Opt. **12,** 095704 (2010).
6. W. W. Simmons, D. R. Speck, and J. T. Hunt, Appl. Opt. **17,** 999 (1978).
7. J. T. Hunt, J. A. Glaze, W. W. Simmons, and P. A. Renard, Appl. Opt. **17,** 2053 (1978).
8. B. M. Van Wonterghem, J. R. Murray, J. H. Campbell, D. R. Speck, C. E. Barker, I. C. Smith, D. F. Browning, and W. C. Behrendt, Appl. Opt. **21,** 4932 (1997).
9. J. E. Murray, D. Milam, C. D. Boley, K. G. Estabrook, and J. A. Caird, Appl. Opt**. 39,** 1405 (2000).
10. J. T. Hunt, "National ignition facility performance review 1999", (California: University of California Livermore, 2000).
11. J. H. Campbell, R. A. Hawley-Fedder, C. J. Stolz, J. A. Menapace, M. R. Borden, P. K. Whitman, J. Yu, M. J. Runkel, M. O. Riley, M. D. Feit, and R. P. Hackel, Proc. SPIE **5341,** 84 (2004).
12. D. Liu, F. Lv, J. Cao, R. Xu, J. Zhu, D. Fan, J. Xiao, and X. Zhou, Chin. Opt. Lett. **4,** 601 (2006).
13. A. K. Potemkin, T. V. Barmashova, A. V. Kirsanov, M. A. Martyanov, E. A. Khazanov, and A. A. Shaykin, Appl. Opt. **46,** 4423 (2007).
14. T. Peng, J. Zhao, L. Xie, Z. Ye, H. Wei, J. Su, and J. Zhao, Appl. Opt. **46,** 3205 (2007).
15. B. Kang, G. T. Joo, and B. K. Rhee, J. Kor. Phys. Soc. **56,** 325 (2010).